

# Effects of Thermal-Infrared Emissivity Directionality on Surface Broadband Emissivity and Longwave Net Radiation Estimation

Jie Cheng, *Member, IEEE*, and Shunlin Liang, *Fellow, IEEE*

**Abstract**—Directionality is ignored in the satellite retrieval of surface thermal-infrared emissivity, which will unavoidably affect the estimates of surface broadband emissivity and surface longwave net radiation. The purpose of this work is to quantify the effects of emissivity directionality. First, three types of emissivity data are used to calculate hemispherical emissivity and the difference between directional broadband emissivity and hemispherical broadband emissivity. The emissivity directionality is highly significant, and the directional emissivity decreases with increasing view angles. A view angle within  $45^{\circ}$ – $60^{\circ}$  can be found whose directional emissivity is highly close to the hemispherical emissivity, and the difference between the calculated directional and hemispherical broadband emissivity is zero. The difference between the atmospheric downward radiation and blackbody radiation at surface temperature is then determined by extensive simulations. Finally, the error ranges of surface longwave net radiation are presented. If the sensor scan angle is within  $\pm 55^{\circ}$ , the error can reach as high as  $17.48$  and  $14.05$   $\text{W/m}^2$  for water and bare ice, respectively; the error is less than  $2.74$   $\text{W/m}^2$  for snow with different radii; the error can reach  $4.11$   $\text{W/m}^2$  for sun crust; the error is less than  $5.14$   $\text{W/m}^2$  for minerals, sand, slime and gravel; and clay has the smallest error at  $1.02$   $\text{W/m}^2$ .

**Index Terms**—Broadband emissivity, directional emissivity, energy budget, hemispherical emissivity, radiation budget.

## I. INTRODUCTION

SURFACE emissivity has been widely used in many disciplines [1]. Surface broadband (window) emissivity is a key variable for calculating the surface radiation budget [2]. Due to the lack of adequate observations, land surface models adopt a constant emissivity value or a simple parameterization scheme [3]. Remote sensing can provide a more realistic broadband emissivity, which significantly improves the simulation results of land surface models [4]. Many studies have examined the production of a broadband emissivity data set using various

methods [5]. A high spatial-temporal long-term global land surface broadband emissivity data set was recently produced using our newly developed methods and freely released to the public [5]–[7]. In all these broadband emissivity data sets, emissivity directionality is neglected, i.e., broadband emissivity is calculated from the emissivity derived from the satellite observations at a certain view angle. Emissivity directionality has long been recognized by the remote sensing community [8], [9].

The satellite retrieval of surface emissivity is a difficult issue. Surface temperature and emissivity are coupled together provided that the atmosphere effects are correctly removed. It is necessary to compromise and make certain assumptions in surface emissivity retrieval, e.g., ignoring the emissivity directionality. For example, a surface is assumed to be Lambertian in the derivation of operational surface temperature and thermal infrared emissivity products from ASTER and MODIS. Theoretically, hemispherical broadband emissivity is required in calculating surface longwave net radiation. It is evident that the use of directional broadband emissivity will affect the accuracy of surface longwave net radiation estimation. The purpose of this letter is to quantify the effects of the directionality of thermal-infrared emissivity on the calculation of hemispherical broadband emissivity and the errors in calculating surface longwave net radiation. The rest of this letter is arranged as follows: Section II introduces the data used, the methods of the emissivity spectra simulation, and the calculation of broadband emissivity and surface longwave net radiation. Section III presents the effects of emissivity directionality on the estimation of broadband emissivity and surface net longwave radiation. A brief conclusion and discussion are provided in Section IV.

## II. DATA AND METHOD

### A. Refractive Index

The refractive index is used as an input to the Mie code for calculating the single-scattering parameters (single scattering albedo and asymmetry factor) of a particulate within a layered medium. The refractive index used in this study is the same as that in [7], including that of water, ice, and minerals. The spectral range is limited to  $2.5$ – $200$   $\mu\text{m}$  in the simulation.

### B. In-Situ Measurements

There are two types of measurements. The first is the field-measured thermal-infrared angular emissivity spectra of a snow surface composed of different particle radii and the emissivity

Manuscript received March 31, 2013; revised May 14, 2013; accepted June 15, 2013. Date of publication July 19, 2013; date of current version November 25, 2013. This work was supported in part by the National Natural Science Foundation of China under Grants 40901167 and 41001250, by the National High Technology Research and Development Program of China under Grant 2009AA122100, and by the Fundamental Research Funds for the Central Universities of China under Grant 14CX02039A.

J. Cheng is with the State Key Laboratory of Remote Sensing Science, College of Global Change and Earth System Science, Beijing Normal University, Beijing 100875, China (e-mail: brucechan2003@126.com).

S. Liang is with the State Key Laboratory of Remote Sensing Science, College of Global Change and Earth System Science, Beijing Normal University, Beijing 100875, China and also with the Department of Geography, University of Maryland, College Park, MD 20742 USA.

Color versions of one or more of the figures in this paper are available online at <http://ieeexplore.ieee.org>.

Digital Object Identifier 10.1109/LGRS.2013.2270293

spectra of bare ice [10]. The emissivity spectra (8–13  $\mu\text{m}$ ) are measured at  $0^\circ$ – $75^\circ$  (at 15 increments). The accumulated errors of the emissivity measurements are reported to be on the order of 0.01 for most wavelengths. For information on snow particle size, snow characterization and field measurements, please refer to [10]. The second type of measurement is the directional emissivity of water, clay, sand, slime, and gravel measured at  $0^\circ$ – $65^\circ$  (at 5 increments) [11]. The reported measurement accuracy is 0.005.

### C. Emissivity Spectra Simulation

First, the refractive index is used to calculate the single-scattering parameters using Mie code. The radii for snow particles are set as 40 and 300  $\mu\text{m}$ , respectively. The radius for minerals is set to 300  $\mu\text{m}$ . Then, the single-scattering parameters are modified by diffraction subtraction and structure factor correction for radii of 40 and 300  $\mu\text{m}$ , respectively, to consider the packing status [12]. Finally, the single-scattering parameters are used as inputs to the Hapke emissivity model [13] to simulate the directional emissivity at viewing angles of  $0^\circ$ – $85^\circ$  ( $5^\circ$  increments). Given the refractive index of water, the Fresnel Equation is used to calculate the surface directional emissivity ( $0^\circ$ – $85^\circ$ ,  $5^\circ$  increments).

### D. Calculation of Broadband Emissivity and Surface Longwave Net Radiation

The hemispherical emissivity is defined as follows [13]:

$$\varepsilon(h, \lambda) = 2\pi \int_0^1 \varepsilon(\mu, \lambda) \mu d\mu \quad (1)$$

where  $\mu$  is the cosine of the view angle,  $\lambda$  is the wavelength, and  $\varepsilon(\mu, \lambda)$  is the directional emissivity. The broadband emissivity can be denoted as follows:

$$\varepsilon_{bb} = \frac{\int_{\lambda_1}^{\lambda_2} \varepsilon(\lambda) B(\lambda, T_s) d\lambda}{\int_{\lambda_1}^{\lambda_2} B(\lambda, T_s) d\lambda} \quad (2)$$

where  $\lambda_1$  and  $\lambda_2$  are the upper and lower bounds of integration,  $B(\lambda, T_s)$  is the Planck function at surface temperature  $T_s$ . If the emissivity used in (2) is hemispherical emissivity, then the calculated broadband emissivity is denoted as hemispherical broadband emissivity. Accordingly, the calculated broadband emissivity is denoted as directional broadband emissivity given the directional emissivity. The surface longwave net radiation can be written as

$$L_n = \int_{\lambda_1}^{\lambda_2} \varepsilon_\lambda [B(T_s) - L_{a\lambda}] d\lambda = \varepsilon_{bb} (\sigma T_s^4 - L_a) \quad (3)$$

where  $L_{a\lambda}$  is the surface downward longwave radiation,  $L_a$  is the wavelength integration of  $L_{a\lambda}$ , and  $\sigma$  is the Stefan-Boltzmann constant ( $5.67 \times 10^{-8} \text{ W} \cdot \text{m}^{-2} \cdot \text{K}^{-4}$ ). The measured and simulated emissivities in Section II are used to calculate the broadband emissivity in their respective windows using (2). The surface temperature is set to 300 K. The latest Thermodynamic Initial Guess Retrieval (TIGR) database are

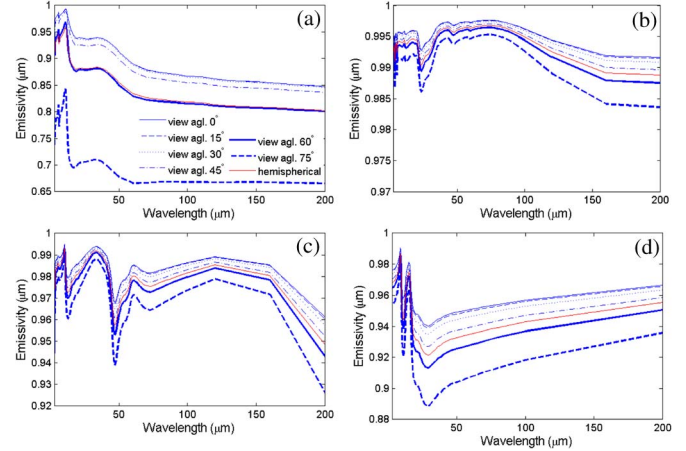


Fig. 1. Simulated directional and derived hemispherical emissivity spectra for (a) water; (b) fine snow; (c) medium snow; and (d) one mineral.

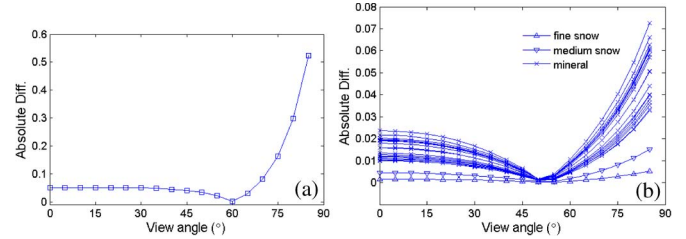


Fig. 2. Absolute differences between the directional and derived hemispherical broadband emissivities of (a) water and (b) snow and mineral.

used to simulate the surface downward longwave radiation [14]. We used the MODTRAN 4.0 code to simulate the directional atmospheric downward radiance in the 0.2–1000  $\mu\text{m}$  spectral range at  $5^\circ$  intervals. Assuming that the directional atmospheric downward radiation is independent of the azimuth angle, we calculate the  $L_{a\lambda}$  by integration. The integration of  $L_{a\lambda}$  in the 0.2–1000  $\mu\text{m}$  spectral range is approximated as that integrated in all wavelengths to balance accuracy and computation time. Surface temperatures are specified as  $T_a - 10$ ,  $T_a - 5$ ,  $T_a$ ,  $T_a + 5$ ,  $T_a + 10$  and  $T_a + 15$ , respectively, where  $T_a$  is the near-surface air temperature of the TIGR atmosphere profiles.

## III. RESULTS AND DISCUSSION

### A. Effects on Broadband Emissivity Estimation

Fig. 1 shows the simulated directional emissivity spectra of water, fine snow (40  $\mu\text{m}$ ), medium snow (300  $\mu\text{m}$ ) and minerals alongside their hemispherical emissivity spectrum derived by (1). The directional emissivity spectra decreases with the increasing view angles, and the hemispherical emissivity spectrum lies between the directional emissivity spectra at view angles of  $45^\circ$  and  $60^\circ$ . We calculated directional broadband emissivity and hemispherical broadband emissivity using (2). We then calculated the differences between the directional and hemispherical broadband emissivity. The calculated hemispherical broadband emissivities are 0.911, 0.994, 0.982, and 0.932 for water, fine snow, medium snow, and minerals, respectively. The absolute difference is shown in Fig. 2. Water has the largest difference, snow has the smallest difference, and minerals have a moderate difference. For water, the absolute difference

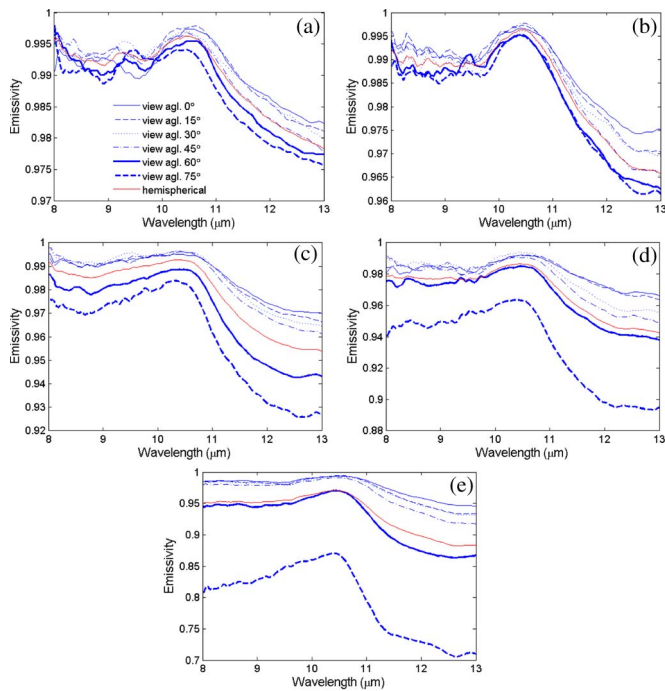


Fig. 3. Field-measured directional emissivity spectra and calculated hemispherical emissivity spectrum for (a) fine dendrite snow; (b) medium grain snow; (c) coarse granular snow; (d) sun crust; (e) bare ice.

reaches the minimum value of 0.001 when the view angle is 60°. The absolute difference ranges from 0.001 to 0.524 for all view angles. For snow, the absolute difference reaches zero when the view angle is 50° and 55°. The difference for all the view angles is less than 0.01. Regarding the minerals, the absolute difference reaches the minimum value of 0.001 when the view angle is 50°. The absolute difference ranges from 0.001 to 0.047.

Fig. 3 shows the field-measured bare ice and snow directional emissivity spectra in the 8–13 μm as well as the corresponding hemispherical emissivity spectra. In the 8–10 μm, the differences between measured directional emissivities are quite small when the view angle is less than 60°, and the angular dependence of directional emissivity cannot be observed from these plots. The angular dependence is highly evident in the 10.5–13 μm. Similar to that shown in Fig. 1, the hemispherical emissivity spectrum lies between the directional emissivity spectra for view angles of 45° and 60°. The calculated hemispherical broadband emissivities are 0.99, 0.985, 0.979, 0.97, and 0.937 for fine dendrite snow, medium grain snow, coarse granular snow, sun crust and bare ice, respectively. The absolute difference is shown in Fig. 4. Bare ice has the largest difference, while the differences for snow are relatively small and increase with increased particle radius. The difference reaches the minimum value when the view angle is 60° for ice and sun crust, whereas the view angle is 45° for the three snow types. The absolute difference ranges from 0.011 to 0.038 for ice, from 0.001 to 0.018 for snow, and from 0.003 to 0.035 for sun crust.

The field-measured directional emissivity in the 8–14 μm spectral range for the different surface types is shown in Fig. 5. The directional emissivity decreases gradually with the increasing view angles. The angular variation is relatively small compared with the previous results except for water. Note

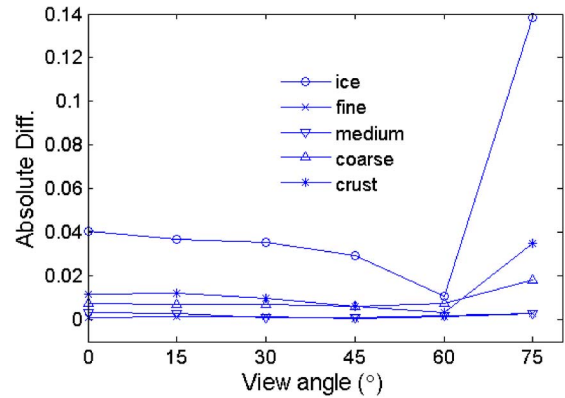


Fig. 4. Absolute difference between the directional broadband emissivities and the derived hemispherical emissivity spectra for ice and snow.

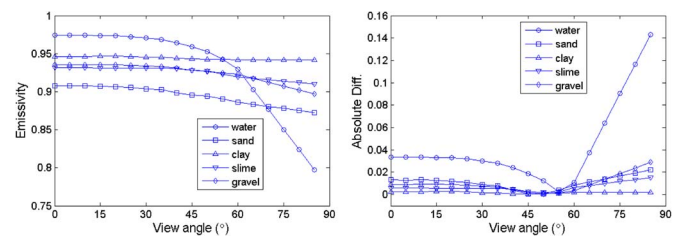


Fig. 5. Angular variation of field-measured direction emissivity (left, after Sobrino and Cuenca, 1999) and the absolute difference between the directional and hemispherical emissivity (right).

that there is only one band in the 8–14 μm spectral range. The calculated hemispherical broadband emissivities are 0.94, 0.895, 0.944, 0.925, and 0.926 for water, sand, clay, slime and gravel, respectively. The difference reaches the minimum value when the view angle is 55° for water and sand, and the view angle is 50° for the remaining three samples. The absolute difference ranges from 0.002 to 0.143 for water, from 0.000 to 0.003 for clay, and from 0.001 to 0.029 for sand, slime and gravel.

According to the aforementioned simulated and measured emissivity data, the angular variation emissivity of the water surface is the largest. The difference between the directional and hemispherical broadband emissivities is also the largest compared with that of the other samples. Fortunately, the water emissivity can be simulated with high accuracy [15] and will not incur large errors on surface longwave net radiation estimation. The angular variation and difference between the directional and hemispherical broadband emissivities for bare ice follow closely behind water. The emissivity angular variation of minerals, slime, and gravel is not as large as that for water and bare ice, but it is also significant. Clay has the smallest emissivity angular variation. The broadband emissivity derived from the simulated and measured emissivities of the snow surface with the same particle radii agree well, with a difference less than 0.004. The difference between the directional and hemispherical broadband emissivities is less than 0.01 and 0.018 for the simulated and measured snow emissivities, respectively. It is evident that we can find a view angle whose directional emissivity is very close to the hemispherical emissivity, and the difference between the calculated directional and hemispherical broadband emissivity is zero. According to the cases in this study, this view angle lies between 45° and 60°.

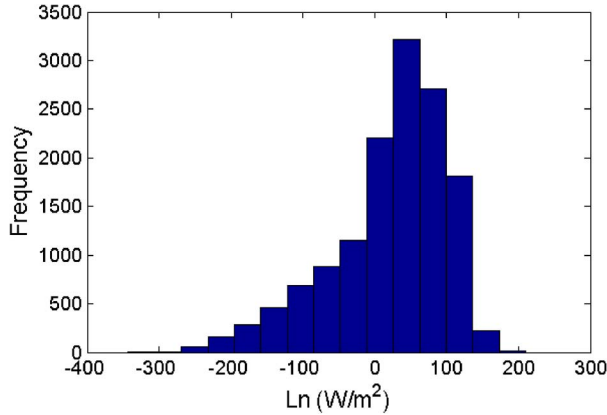


Fig. 6. Histogram of simulated  $\sigma T_s^4 - L_a$ .

### B. Effects on Surface Longwave Net Radiation Estimation

Note that the spectral ranges of the three emissivity sources are different. According to the study of Cheng *et al.* [7], broadband emissivity at 8–13.5  $\mu\text{m}$  can represent broadband emissivity in all wavelengths in surface longwave net radiation estimation. Therefore, we will not strengthen the emissivity spectral range in the estimates of surface longwave net radiation. Instead of calculating surface longwave net radiation, we calculated the  $\sigma T_s^4 - L_a$  in (3) because the error in surface longwave net radiation is proportional to the error in broadband emissivity. Given the broadband emissivity error, we can directly calculate the error in surface longwave net radiation. The histogram of the simulated  $\sigma T_s^4 - L_a$  is shown in Fig. 6. The mean value is 21.69  $\text{W/m}^2$ , and the absolute value changes from zero to 342.75  $\text{W/m}^2$ . Certainly, an error of 0.1 in broadband emissivity corresponds to the error between zero and 34.28  $\text{W/m}^2$  in surface longwave net radiation. This value depends on the atmospheric and surface conditions. In the satellite retrieval or field measurements of surface emissivity, we derived the simplified radiative transfer equation by assuming that the land surface is Lambertian or that the atmospheric downward radiance is isotropic. Regardless of which assumption is adopted, the measured parameter is the directional radiance. In the laboratory measurement, we measured the hemispherical–directional reflectance (the incident angle of the light source is usually  $10^\circ$ ) with the help of an integration sphere, and then we calculated the directional emissivity using Kirchhoff’s law. Therefore, the retrieved surface emissivity is directional. For ASTER, the scan angle is very small. The angle of the retrieved directional emissivity could be approximated as  $0^\circ$ . The scan angle can reach  $\pm 55^\circ$  for MODIS, and the angle of the retrieved directional emissivity should be  $0^\circ$ – $55^\circ$  without considering the topography. Assuming directional broadband emissivities derived from ASTER and MODIS emissivity products have the same accuracy, the accuracy of surface longwave net radiation using MODIS emissivity will be better than that estimated with the ASTER emissivity product because the absolute difference between the directional and hemispherical broadband emissivities decreases with an increasing view angle until it reaches zero. Table I presents the error range when the directional broadband emissivity at the  $0^\circ$ – $55^\circ$  view angle is used to replace the hemispherical broadband emissivity to calculate surface longwave net radiation. The error can reach as high as 17.48 and 14.05  $\text{W/m}^2$  for water and bare ice,

TABLE I  
ERROR RANGE OF CALCULATING SURFACE LONGWAVE NET RADIATION  
WITH THE DIRECTIONAL BROADBAND EMISSIVITY AT  $0^\circ$ – $55^\circ$   
VIEW ANGLE ( $\text{W/m}^2$ )

Simulated emissivity spectra				
water		snow		minerals
0-17.48		0-1.02		0-5.14
Hori et al. emissivity spectra				
Bare ice	Fine snow	Medium snow	Coarse snow	Sun crust
0-14.05	0-2.74	0-1.02	0-2.74	0-4.11
Sobrino et al. emissivity				
water	sand	clay	slime	gravel
0-11.65	0-4.46	0-1.02	0-2.06	0-3.08

respectively; the error is less than 2.74  $\text{W/m}^2$  for snow with different radii; the error can reach 4.11  $\text{W/m}^2$  for sun crust; the error is less than 5.14  $\text{W/m}^2$  for minerals, sand, slime and gravel; and clay has the smallest error of 1.02  $\text{W/m}^2$ .

### IV. CONCLUSION AND DISCUSSIONS

Surface broadband emissivity in the thermal infrared region is essential for calculating surface longwave net radiation. Satellite-retrieved surface emissivity has directionality, which will inevitably produce errors in the estimates of surface longwave net radiation if ignored. The simulated and measured directional emissivities are used to investigate the effects of emissivity directionality on broadband emissivity calculation. The directional emissivity spectra decrease with an increasing view angle. Water has the largest angular variation, and bare ice follows closely behind. The emissivity angular variation of minerals, sand, slime, and gravel is not as large as that for water and bare ice but is also significant. Clay has the smallest angular variation emissivity. The behavior of the difference between the directional and hemispherical broadband emissivities is highly similar to that of the emissivity angular variation. The absolute difference can reach as high as 0.524 and 0.138 for water and bare ice, respectively. The maximum absolute differences are 0.015, 0.018, 0.022, 0.035, and 0.047 for slime, snow, sand, sun crust, and minerals, respectively. The maximum absolute difference is only 0.003 for clay. We found a view angle within  $45^\circ$ – $60^\circ$  whose directional emissivity is highly close to the hemispherical emissivity, and the difference between the calculated directional and hemispherical broadband emissivities is zero. By virtue of the latest TIGR database and the MODTRAN 4.0, we calculated the possible range of  $\sigma T_s^4 - L_a$  through extensive simulation. According to the absolute difference between the directional and hemispherical broadband emissivities, we present the error bounds of surface longwave net radiation. If the sensor angle can reach  $\pm 55^\circ$  like MODIS, the error can be as high as 17.48 and 14.05  $\text{W/m}^2$  for water and bare ice, respectively; the error is less than 2.74  $\text{W/m}^2$  for snow

with different radii; the error can reach  $4.11 \text{ W/m}^2$  for sun crust; the error is less than  $5.14 \text{ W/m}^2$  for minerals, sand, slime and gravel; and clay has the smallest error, at  $1.02 \text{ W/m}^2$ .

Currently, measurements of angular variation emissivity are very scarce. Only a limited number of simulated and measured emissivities are used in this study. A typical landscape, i.e., a soil-vegetation system, is not considered. Usually, we would use the radiative transfer model or the geometrical model to simulate the directional emissivity [9]. However, the emissivity or reflectance of the component is assumed to be Lambertian in these models. Furthermore, these models lack validation, as field measurements over vegetation canopies are rarely available. Further studies on measuring the directional emissivity of various natural land surfaces, especially a soil-vegetation system, at broadband spectral ranges are needed. Direct measurement method is commonly used to obtain the emissivity of natural surfaces for its greater flexibility. In the direct measurement of surface emissivity, the directionality of the surface properties or the background radiation is ignored, i.e., either that the surface is assumed as a perfectly diffuse reflector or the background radiation is assumed as a diffuse (independent of direction). In reality, both assumptions are hard to meet and will bring systematic errors in the derived surface emissivity. Kribus *et al.* thoroughly discussed the systematic errors in the direct emissivity measurements caused by directional effects and presented some recommendations for improving experimental procedures in emissivity measurement [16]. As pointed out by Kribus *et al.*, in some situations, the systematic error is much larger than the 0.01–0.02 typical error values reported in the literature, which is based on the inherent errors of the equipment used and on the data scatter that is observed when the experiment is repeated. Therefore, we must pay attention to each procedure that could introduce errors in the direct measurement of surface emissivity.

Because the observational angles of satellite sensors are limited, it is difficult to calculate the hemispherical emissivity using the retrieved directional emissivity. A practical way to improve the estimates of broadband emissivity is to improve and develop versatile radiative transfer models that can characterize the angular distribution of emissivity for typical land surface types. With these models, we can either establish the relationship between hemispherical broadband emissivity and broadband emissivity at a certain angle or simulate the hemispherical broadband emissivity provided with surface characteristics.

## REFERENCES

- [1] J. Cheng, S. Liang, Q. Liu, and X. Li, "Temperature and emissivity separation from ground-based MIR hyperspectral data," *IEEE Trans. Geosci. Remote Sens.*, vol. 49, no. 4, pp. 1473–1484, Apr. 2011.
- [2] S. Liang, K. Wang, X. Zhang, and M. Wild, "Review of estimation of land surface radiation and energy budgets from ground measurements, remote sensing and model simulation," *IEEE J. Sel. Topics Earth Observ. Remote Sens.*, vol. 3, no. 3, pp. 225–240, Sep. 2010.
- [3] G. B. Bonan, K. W. Oleson, M. Vertenstein, S. Levis, X. Zeng, Y. Dai, R. E. Dickinson, and Z.-L. Yang, "The land surface climatology of the community land model coupled to the NCAR community climate model," *J. Climate*, vol. 15, no. 22, pp. 3123–3149, Nov. 2002.
- [4] M. Jin and S. Liang, "An improved land surface emissivity parameter for land surface models using global remote sensing observations," *J. Climate*, vol. 19, no. 12, pp. 2867–2881, Jun. 2006.
- [5] J. Cheng and S. Liang, "Estimating global land surface broadband thermal-infrared emissivity from the advanced very high resolution radiometer optical data," *Int. J. Digit. Earth*, 2013, to be published.
- [6] H. Ren, S. Liang, G. Yan, and J. Cheng, "Empirical algorithms to map global broadband emissivities over vegetated surfaces," *IEEE Trans. Geosci. Remote Sens.*, vol. 51, no. 5, pp. 2619–2631, May 2013.
- [7] J. Cheng, S. Liang, Y. Yao, and X. Zhang, "Estimating the optimal broadband emissivity spectral range for calculating surface longwave net radiation," *IEEE Geosci. Remote Sens. Lett.*, vol. 10, no. 2, pp. 401–405, Mar. 2013.
- [8] Y. Du, Q.-H. Liu, L.-F. Chen, Q. Liu, and T. Yu, "Modeling directional brightness temperature of the winter wheat canopy at the ear stage," *IEEE Trans. Geosci. Remote Sens.*, vol. 45, no. 11, pp. 3721–3739, Nov. 2007.
- [9] J. A. Sobrino, J. C. Jimenez-Munoz, and W. Verhoef, "Canopy directional emissivity: Comparison between models," *Remote Sens. Environ.*, vol. 99, no. 3, pp. 304–314, Nov. 2005.
- [10] M. Hori, T. Aoki, T. Tanikawa, H. Motoyoshi, A. Hachikubo, K. Sugiura, T. J. Yasunari, H. Eide, R. Stovold, Y. Nakajima, and F. Takahashi, "In-situ measured spectral directional emissivity of snow and ice in the 8–14  $\mu\text{m}$  atmospheric window," *Remote Sens. Environ.*, vol. 100, no. 4, pp. 486–502, Feb. 2006.
- [11] J. A. Sobrino and J. Cuenca, "Angular variation of thermal infrared emissivity for some natural surfaces from experimental measurements," *Appl. Opt.*, vol. 38, no. 18, pp. 3931–3936, Jun. 1999.
- [12] J. Cheng, S. Liang, F. Weng, J. Wang, and X. Li, "Comparison of radiative transfer models for simulating snow surface thermal infrared emissivity," *IEEE J. Sel. Topics Earth Observ. Remote Sens.*, vol. 3, no. 3, pp. 323–336, Sep. 2010.
- [13] B. Hapke, *Theory of Reflectance and Emittance Spectroscopy*. New York, NY, USA: Cambridge Univ. Press, 1993.
- [14] A. Chedin, N. A. Scott, C. Wahiche, and P. Moulinier, "The improved initialization inversion method: A high resolution physical method for temperature retrievals from satellites of the TIROS-N series," *J. Climate Applied Meteorol.*, vol. 24, no. 2, pp. 128–143, Feb. 1985.
- [15] K. Masuda, T. Takashima, and Y. Takayama, "Emissivity of pure and sea waters for the model sea surface in the infrared window regions," *Remote Sens. Environ.*, vol. 24, no. 2, pp. 313–329, Mar. 1988.
- [16] A. Kribus, I. Vishnevetsky, E. Rotenberg, and D. Yakir, "Systematic errors in the measurement of emissivity caused by directional effects," *Appl. Opt.*, vol. 42, no. 10, pp. 1839–1846, Apr. 2003.